Climate Dynamics manuscript No.
(will be inserted by the editor)

Sudden stratospheric warmings and tropospheric blockings in a multi-century simulation of the IPSL-CM5A coupled climate model

Jessica Vial · Tim J. Osborn · François Lott

Received: date / Accepted: date

Abstract The relation between Sudden Stratospheric Warmings (SSWs) and blocking events is analyzed in a multi-centennial pre-industrial simulation of the Institut Pierre Simon Laplace coupled model (IPSL-CM5A), prepared for the fifth phase of the Coupled Model Intercomparison Project (CMIP5). The IPSL model captures a fairly realistic distribution of both SSWs and tropospheric blocking events, albeit with a tendency to overestimate the frequency of blocking in the western Pacific and underestimate it in the Euro-Atlantic sector.

The 1000-year long simulation reveals statistically significant differences in blocking frequency and duration over the 40-day periods preceding and following the onset of SSWs. More specifically, there is an enhanced blocking frequency over Eurasia before SSWs, followed by an westward displacement of blocking anomalies over the Atlantic region as SSWs evolve and then decline. The frequency of blocking is reduced over the western Pacific sector during the life-cycle of SSWs, while the model simulates no significant relationship with eastern Pacific blocks. Finally, these changes in blocking frequency tend to be associated with a shift in the distribution of blocking lifetime toward longer-lasting blocking events before the onset of SSWs and shorter-lived blocks after the warmings.

This study systematically verifies that the results are consistent with the two pictures that (i) blockings produce planetary scale anomalies that can force vertically propagating Rossby waves and then SSWs when the waves break and (ii) SSWs affect blockings in return, for instance via the effect they have on the North Atlantic Oscillation (NAO).

Keywords Stratosphere-troposphere interaction · atmospheric blocking · sudden stratospheric warming · multi-century climate simulation · Northern Hemisphere · Blocking frequency · Blocking duration · Blocking location

1 Introduction

The dynamical linkage between sudden stratospheric warmings (SSWs) and tropospheric blockings is in good part related to vertically propagating planetary waves (PWs), which are known to drive SSWs through wave mean flow interaction (Matsuno, 1971). In these processes, the role of PWs with zonal wavenumber 1 and 2 is dominant, and their tropospheric signature is particularly pronounced during blocking events (Martius et al, 2009; Naujokat et al, 2002; Nishii et al, 2011; Quiroz, 1986; Tung and Lindzen, 1979). For instance, Quiroz (1986) found that blocking events precede weak vortex events by around 3-4 days in 85% of the 20 wintertime cases he examined for the period 1981-1985. This lead-lag relation was also suggested by Naujokat et al (2002), who found that in the three major SSWs considered, which occurred in December 1987, 1988 and 2001, all were preceded by strong blocking episodes over the North Atlantic, 1 to 2 weeks prior to the warmings.

When longer datasets were analyzed, more detailed studies based on reanalysis and on model simulations emphasized the importance of the regional location of blocking for the onset and type of SSWs. For instance, Martius et al (2009)'s analysis based on the ERA-40 reanalysis dataset for the period 1957-2001

Jessica Vial
LMD (Laboratoire de Météorologie Dynamique), Université Pierre et Marie Curie (UPMC), 4 place Jussieu, 75752 Paris cedex 05, France
E-mail: jessica.vial@lmd.jussieu.fr

Tim J. Osborn
Climatic Research Unit, School of Environmental Sciences, University of East Anglia, Norwich NR4 7TJ, United Kingdom

François Lott
LMD, Ecole Normale Supérieure (ENS), 24 rue Lhomond, 75231 Paris cedex 05, France

revealed that SSWs due to stratospheric vortex displacements are mostly preceded by Atlantic blocks while SSWs due to stratospheric vortex splitting are more likely to occur when there are blockings over both the Atlantic and the Pacific simultaneously, or over the eastern Pacific region only. Other studies, based on re-analysis datasets and on model simulations (up to three hundred years long), have shown that anomalous blockings over the Euro-Atlantic/Eurasian sector can reinforce the corresponding ridge in the steady PW prior to the onset of SSWs (Kolstad and Charlton-Perez, 2011; Nishii et al, 2011; Woollings et al, 2010). Within the same line of thought, it happens that western Pacific blocking occurs near a trough of the steady PWs; this can in fact yield a weaker PW forcing by reducing the PW amplitude within the troposphere, and induce a stratospheric cooling (Nishii et al, 2011). These results emphasize the significance of the location of tropospheric blockings on the SSW properties and onset.

The fact that there is also an influence of SSWs on blockings at a later stage has also been established by various authors (Kodera and Chiba, 1995; Labitzke, 1965; Thompson and Wallace, 2000; Woollings et al, 2010). This mostly concerns Euro-Atlantic blocks, which generally occur during the negative phase of the Arctic Oscillation (AO-, Thompson and Wallace, 2000) and of the North Atlantic Oscillation (NAO-, Ambaum and Hoskins, 2002; Baldwin and Dunkerton, 2001).
To explain how there can be enhanced blockings after SSWs, blocking being often associated with increased PWs in the troposphere, while PWs are reduced in the stratosphere after a SSW, there are at least two possibilities. The first is that during the mature phase of SSWs, there are easterly and weak westerly winds in the stratosphere, which prevent further upward propagation of stationary PWs (Charney and Drazin, 1961), even if there is strong tropospheric forcing. The second is that blockings are not always yielding to an enhanced PW flux toward the stratosphere. The second factor could have a regional origin, as was suggested for the case of the Pacific blockings. It could also be related to the duration of blockings (Martius et al, 2009; Quiroz, 1986), in the sense that shorter lasting blocks produce shorter-living upward wave packets that are less efficient in producing SSWs than longer blocks (Harnik, 2009).

One difficulty in settling these issues is that the relationship between SSWs and blockings is relatively subtle, relative to the amount of natural variability. The relations between SSWs and blockings discussed before are questioned by some authors, simply because they are not very robust to changes in the ways SSWs and blockings are defined (Baldwin and Thompson, 2009; Barriopedro et al, 2010). In the same line of thought, Taguchi (2008) questions the statistical test generally used to assert the relations between SSWs and blockings, and finds no significant relations when he uses a bootstrap method. Note that the negative result in Taguchi (2008) can also be due to his choice of using the 500-hPa geopotential level to diagnose blockings (Martius et al, 2009; Nishii et al, 2011), but this nevertheless witnesses that the relations are not very strong. Note also that these difficulties are inherently related to the fact that SSWs are quite rare (around six per decades; see in Charlton and Polvani, 2007) and that the reanalysis datasets cover a relatively short period in this respect.

To circumvent these problems, some of the recent experiments done with Earth System Models in the context of the fifth phase of the Coupled Model Intercomparison Project (CMIP5, Taylor et al, 2012) can be very helpful. In fact, these models include necessary (although not sufficient) ingredients that can produce tropospheric blockings with a consistent oceanic response underneath. Some of them, and this is one of the essential improvements made since CMIP3, also include a realistic stratosphere and produce realistic SSWs (Charlton-Perez et al, submitted). In this context, the Institut Pierre Simon Laplace coupled model (IPSL-CM5A) is quite representative of what is done in other groups. With its improved stratosphere as described in Lott et al (2005) and Hourdin et al (2012), it can now be considered as a "high-top" climate model (Charlton-Perez et al, submitted). Also, these models have control simulations that can last a few thousand years, so the sampling problem concerning the number of SSWs does not apply to these simulations.

The purpose of this paper is twofold. The first is to validate the IPSL-CM5A model in terms of its stratospheric dynamics and in terms of blockings. In this context, we will analyze to which extent it produces realistic relationships between SSWs and blockings, and test these relations using bootstrap methods. Second, all along the paper, we will also check some of the known mechanisms at the basis of the relation between blocking, PWs, and the AO using Eliassen-Palm flux diagnostics.
The paper is organized as follows: Section 2 describes the dataset and methodology, and provides a validation of the model to simulate SSWs and tropospheric blockings. Some results concerning the temporal evolution of tropospheric and stratospheric features closely related to blocking are presented in Section 3. The relationship between the occurrence of SSWs and blocking episodes is analyzed in more detail in Section 4, and Section 5 summarizes the results.

2 Data, analysis and model validation

2.1 Data

The model simulation used in this study is the 1000-year (nominally 1800-2799) Pre-industrial Control experiment of the IPSL-CM5A atmosphere-ocean coupled model (Dufresne and al., Submitted; Hourdin et al, 2012; Lott et al, 2005), prepared for CMIP5. Its atmospheric component (LMDZ5) uses a horizontal resolution of 1.9° in latitude and 3.75° in longitude and 39 levels in the vertical (15 levels are above 20 km - ∼50 hPa), with the model lid above the stratopause at ∼65 km (∼0.5 hPa), although most of the mesosphere (between 55 km and 65 km) is occupied by an artificial Rayleigh drag sponge layer that damps the wave and not the mean flow (Lott et al, 2005). Also important for an accurate representation of the large-scale circulation in the stratosphere, the model includes the orographic and non-orographic gravity waves parametrization schemes described in Lott et al (2005).
To validate the model representation of tropospheric blocking and of the stratospheric variability, we also use the 44-year ERA-40 reanalysis dataset (Uppala et al, 2005), provided by the European Centre for Medium-Range Weather Forecasts (ECMWF) at a 2.5° horizontal and 60-level vertical resolution.

2.2 Stratospheric sudden warming

To identify SSWs, we follow Limpasuvan et al (2004), and take for a measure of the strength of the polar vortex the leading principal component (PC) associated with the first empirical orthogonal function (EOF) of the deseasonalized zonal-mean zonal wind anomalies at 10 hPa.
The leading variability pattern associated with the first EOFs from ERA-40 and the models are shown in Figure 1. Overall, both structures are very similar, and represent a dipole pattern with a reversal of sign at about 40°N, and a maximum amplitude (at ∼65°N) of about 11 m/s. The prominent difference, however, is in the subtropical regions (between 20°N and 35°N), where the model underestimates the wind amplitude by about 2 m/s. Also, the variance explained by these EOFs is quite similar (62% in the model versus 59% in the reanalysis).

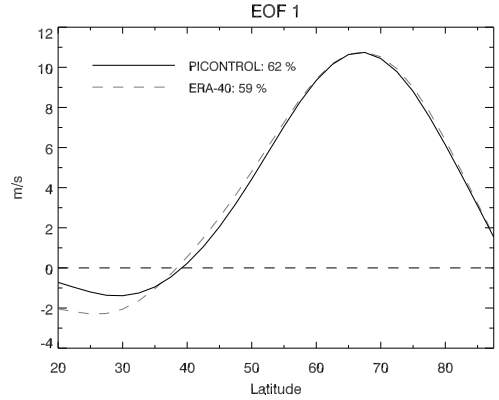

Fig. 1 10-hPa zonal-mean zonal wind structure associated with the first EOF from ERA-40 (dashed grey) and the IPSL-CM5A climate model (solid black). The patterns shown result from the regression of the zonal mean zonal wind onto the first PC.

To identify SSWs we next low-pass filter the PCs using a 15-day boxcar average, and identify the onset as the dates when the filtered PCs drop more than one standard deviation below its climatological mean ($-\sigma$). Here, $\sigma \simeq 18.1 m/s$ for IPSL and $\sigma \simeq 19.1 m/s$ for ERA-40, which indicates that the model captures relatively well the amplitude of the variability in the strength of the polar vortex. Also to ensure statistical independence between the events, we consider that two consecutive onset dates (within one year) must be separated by at least 120 days (the number of the SSWs is only weakly sensitive to that threshold).
In ERA-40, our method selects half of the warmings detected using the World Meteorological Organisation (WMO, Andrews et al, 1987) and listed in Charlton and Polvani (2007). SSWs identified here but not by the WMO approach correspond to jet weakenings that do not strictly correspond to major SSWs. Overall, 672 SSW events are selected in the model (corresponding to ∼ 0.67 events per year), and 34 events are identified in ERA-40 (∼ 0.77 events per year).
The monthly distribution of SSW central dates (the mid-time between the onset and decay dates - the decay date being when the PCs rise above $-\sigma$) for the reanalysis and the model, are shown in Figure 2. In it, we see that SSW activity in ERA-40 increases abruptly in December and decays abruptly after March, as was

shown in Limpasuvan et al (2004); Lott et al (2005), whereas in the model the frequency of SSWs increases and decreases more progressively over a period going from November to April-May, with the highest activity from December to March (i.e., as in ERA-40). This difference with ERA-40 could be interpreted as a model bias, but it could also be related to the larger sample size of the model allowing detection of rarer events that may be absent in ERA-40 due to sampling period (e.g., in November). Note also that during the active period, the model underestimates the total frequency of SSW occurrence by about 10%, and we found that this result showed little sensitivity to the thresholds of the amplitude and duration we have selected, or to the boxcar average.

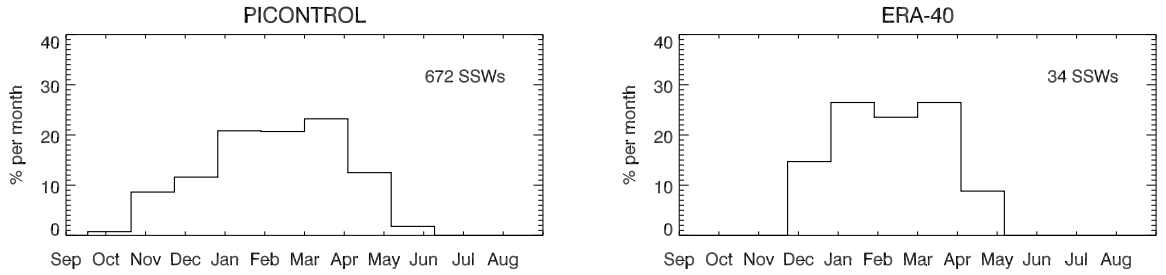

Fig. 2 Left: Monthly frequency of the 672 SSW central dates as simulated by the IPSL-CM5A model from 1 January 1800 to 31 December 2799, computed from the amplitude of the low-pass filtered PC time series. Right: Same as the left panel, but for the 34 SSW central dates as diagnosed from ERA-40.

In the following and to be consistent with the re-analysis, only the SSW events whose onset dates are between the 1^{st} of December to the 31^{st} of March (DJFM) are selected, which reduces the number of SSW events to 480 in the IPSL model.

2.3 Tropospheric blocking

Our blocking detection method combines the traditional approaches employed by Tibaldi and Molteni (1990) and Dole and Gordon (1983), and identifies atmospheric blocking highs when (1) there are easterlies in regions where the jet streams and storm tracks are usually located and (2) there is an anticyclonic circulation on the poleward side of the easterlies.
More specifically blocked days are calculated using the index described in Vial and Osborn (2011), which detects 500 hPa geopotential meridional gradient reversals between two averaged 5-grid latitudinal bands located on each side of a reference latitude. This reference latitude is longitude dependent and corresponds to where the amplitude of the climatological storm track (calculated as the temporal standard deviation of the 2-8 day band-pass filtered geopotential field at 500 hPa) is maximum. This blocking index also requires a positive geopotential height anomaly (i.e., at least one standard deviation above the seasonal mean) on the poleward side of the meridional height reversal (see Vial and Osborn, 2011 for details). A large-scale blocking episode is then defined when a blocking candidate spans at least 15° longitude and persists for at least 5 days.
Finally, in this study, blockings are detected from 1^{st} October to 31^{st} May (ONDJFMAM), since SSWs occurring in DJFM may be associated with tropospheric signals well before and after their onset dates. Here, the 2-month periods preceding and following the onset date of SSW events are inspected.

Unlike our method, which belongs to the traditional approaches that search for meridional gradient height reversal, some other studies use blocking detection methods based on Rossby wave breaking criteria (Martius et al, 2009; Pelly and Hoskins, 2003; Woollings et al, 2010, and see Barriopedro et al, 2010 for a review of blocking indices). We have nevertheless preferred to choose an isobaric set of criteria in part because they refer to purely tropospheric diagnostics and therefore are less biased to emphasize the troposphere-stratosphere linkage than wave breaking diagnostics based on potential vorticity (which detect intrusions of stratospheric air into the troposphere, and therefore have a strong signature throughout the atmosphere).

The blocking frequency during the ONDJFMAM period from the 1000-year model simulation in Fig. 3, exhibits a minimum in autumn and a sharp maximum in late spring over the Euro-Atlantic sector, while in the Pacific region, there is a tendency for more frequent blocks in winter and early spring (December to March) than in the temperate months. These results are in agreement with ERA-40 (right panel) over the Pacific, but differ over the Euro-Atlantic sector, where blockings are more active in DJFM in ERA-40. Another major difference between IPSL-CM5A and ERA-40 is that the model captures blocking episodes

in the western Pacific sector (between 135°E and 195°E) that do not exist in the reanalysis. Overall in the Euro-Atlantic sector, the IPSL model underestimates the frequency of blocking (a common feature in climate models according to D'Andrea et al, 1998; Scaife et al, 2010; Vial and Osborn, 2011), by up to 10% in the winter months, and in addition, incorrectly simulates the seasonal cycle, as seen by differences in the monthly mean blocking statistics in Fig. 3. Over the Pacific, however, the model captures the basic structure of the seasonal cycle (i.e. the same as ERA0-40), despite an overall positive bias.

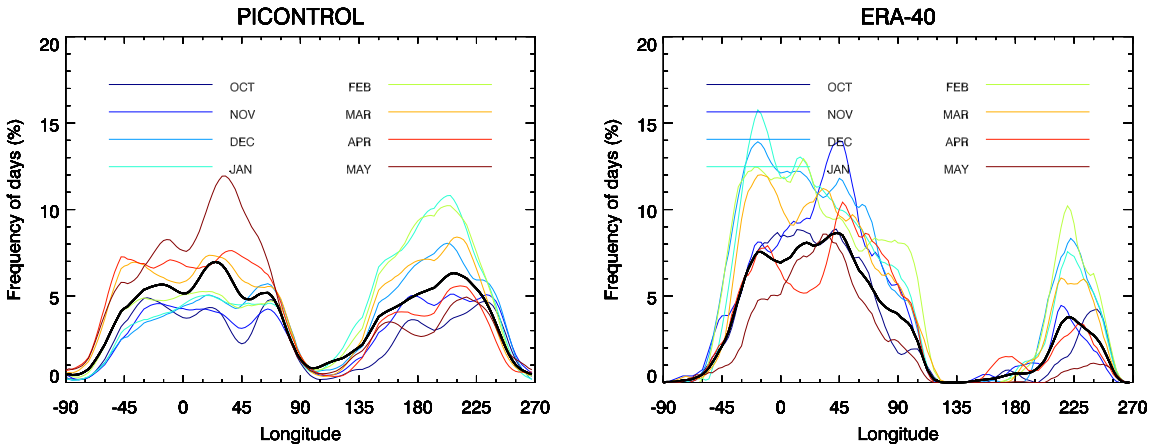

Fig. 3 Frequency of all days that are part of large-scale blocking episodes (at least 5-day duration and 15° longitude extension) as a function of longitude, for the ONDJFMAM period (thick black line), as simulated by IPSL-CM5A (left) and diagnosed from ERA-40 (right). Monthly mean frequencies are displayed by the different colors, as explained in the legend.

3 Temporal evolution of stratospheric sudden warming events

In this section, the temporal evolution of zonal-mean zonal wind, meridional eddy fluxes, PWs and blocking frequency composited for the 480 SSW events are calculated for each calendar day, spanning up to 80 days prior to 80 days following the onset of SSWs. In the remainder of this paper, we refer to the periods preceding and following the onset date of SSWs as PRE-SSW and POST-SSW periods, respectively. All presented fields are anomalies from the daily climatological seasonal cycle calculated from the 1000-year model simulation. The wave quantities presented in this paper (i.e., meridional heat and momentum fluxes and PWs) are calculated as in Pawson and Kubitz (1996).

3.1 Zonal-mean zonal wind

The simulated zonal-mean zonal wind anomalies, averaged between 45°N and 75°N and composited for the 480 SSW events are shown in Figure 4. Black hatching areas indicate that the anomalies are statistically significant at the 99% confidence level, calculated from a T-test. It exhibits a similar picture to that previously reported (Baldwin and Dunkerton, 2001; Limpasuvan et al, 2004), with a rapid weakening of the stratospheric zonal-mean zonal winds propagating down to the troposphere, where anomalous easterly winds then persist for up to two months. As in observations, the rapid breakdown of the stratospheric zonal flow is preceded by anomalously strong westerlies, and is followed by the gradual recovery of the stratospheric polar vortex (Limpasuvan et al, 2004).
Note also that the model simulates the weakest zonal winds about 5 days after the onset date of SSW events, although this feature is sensitive to the wind anomaly threshold used to define the SSW onset dates (i.e., here taken at one standard deviation below the climatological mean).

3.2 Eddy heat flux and blocking

In order to corroborate that in the model the tropospheric forcing and the upward propagation of large-scale PWs are precursors of the SSWs, we follow Polvani and Waugh (2004) and Charlton and Polvani (2007), and calculate the poleward heat flux at 100 hPa averaged between 45°N and 75°N. The composite of this flux for the 480 SSW events at each calendar day within the 60-day PRE-SSW to the

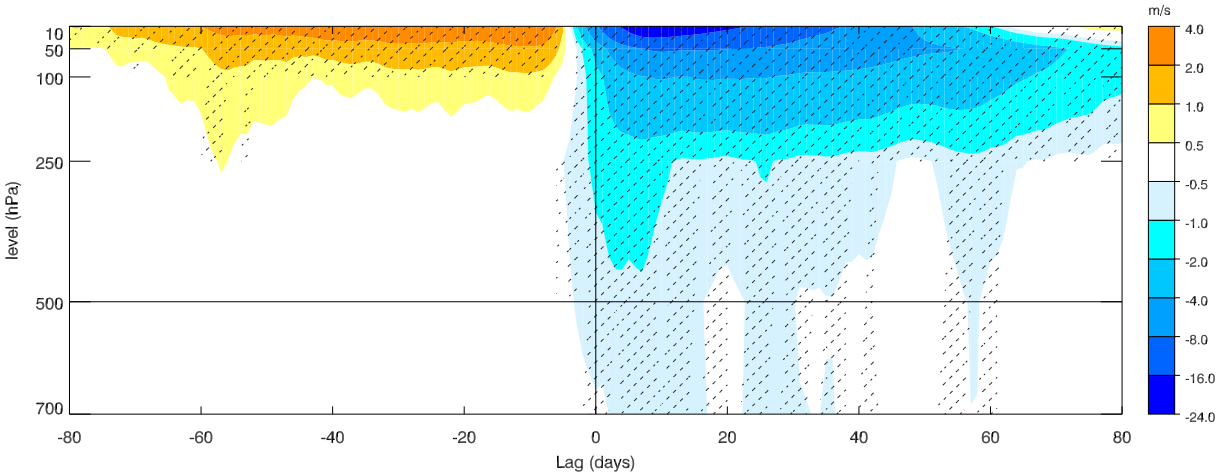

Fig. 4 Temporal evolution of the deseasonalized zonal-mean zonal wind anomalies as a function of pressure (in hPa), averaged between 45°N and 75°N, and composited for the 480 SSW events at each calendar day within the 80-day PRE-SSW to the 80-day POST-SSW period. Significant anomalies at the 99% confidence level (based on a T-test) are indicated with black hatching. These results are derived from the 1000-year IPSL-CM5A model simulation.

60-day POST-SSW window is shown in Fig. 5, where the solid and thick portions of the curves indicate that the anomalous heat fluxes are statistically significant at the 99% level (based on a T-test).
The anomalous heat flux starts being significant about 10 days before the onset of SSWs and increases up to a maximum at about lag = 5 days, when the zonal winds are the weakest (see Fig. 4). Both wavenumbers 1 and 2 contribute to enhanced upward propagation of wave energy (Fig. 5). After lag = 5 days, the anomalous heat flux decreases and becomes negative at lag = 10 days.

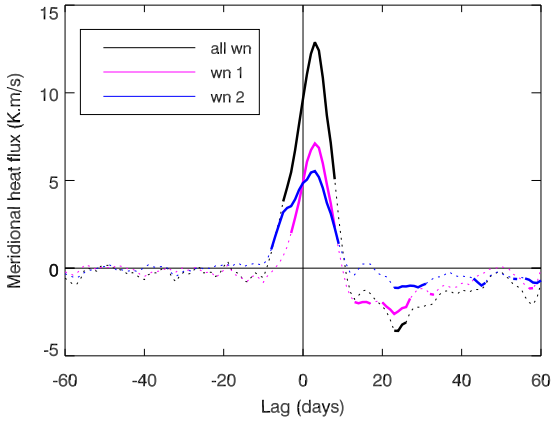

Fig. 5 Temporal evolution of the meridional heat flux ($\overline{v'T'}$) anomalies at 100 hPa, averaged between 45°N and 75°N, where the primes are deviations from the zonal mean due to all wavenumbers (black curve), zonal wavenumber 1 (magenta curve) and zonal wavenumber 2 (blue curve), and the overbar is the zonal mean. Anomalies are computed as deviations from the daily climatological seasonal cycle, and composited for all 480 SSW events at each calendar day within the 60-day PRE-SSW to the 60-day POST-SSW period. Significant anomalies at the 99% confidence level (based on a T-test) are indicated by the thick portions of the curves.

The importance of the geographical location of the tropospheric blockings relative to the phase of the climatological-mean planetary waves for the variability of upward propagating PWs was demonstrated in previous studies (e.g., Martius et al 2009; Nishii et al 2011). It simply follows that when a blocking ridge coincides with a climatological ridge, the PW forcing is reinforced whereas when it coincides with a climatological trough, the PW forcing can be reduced. We largely use this idea in the following and test it with our very long dataset. We also use it to interpret the simulated relationship between blockings and SSWs during both the increase and decay of SSWs, and argue that the reduced vertical flux of wave activity after SSWs may in part be due to changes in the geographical location of blockings.

The longitudinal distribution of the anomalous frequency of blocking days composited for the 480 SSW events is shown in Fig. 6 where the black hatching represents the 99% confidence interval according to a T-test. Figure 6 also displays the sum of the climatological-mean planetary wave 1 to 3 averaged between 45°N and 75°N (grey contours), in order to identify when and where the geographical location of the

blocking anomalies coincide with the phase of the climatological-mean planetary waves.
The eastern parts of the North Atlantic (45°W-0°) and Eurasia (0°-90°E), as well as the North Pacific (135°E-255°E) basins emerge clearly as regions where the anomalies in blocking frequency reach their highest values (Fig. 6). As was previously shown in Section 2, these regions are where blocking events are the most frequent (see also Fig. 3).
Prior to the SSW onset, from lag = -20 days, the frequency of blocking days is enhanced over Eurasia, where a climatological ridge is located. Based on previous studies (e.g., Martius et al 2009; Nishii et al 2011), it is plausible that blockings over this region contribute to the tropospheric forcing of large-scale upward propagating PWs into the stratosphere (as seen by the positive anomalies in the meridional heat flux associated with wavenumber 1 and 2 in Fig. 5), which in turn trigger SSW events.
After the onset of SSWs, positive anomalies in blocking frequency displace progressively over the climatological planetary trough in the Atlantic region, and persist there for about two months (with a rather small but significant signal at lag $\simeq$ 10 to 45 days). These results are consistent with the decay of the wave activity fluxes after the SSW onset date, and the negative anomalies from lag = 10 days (Fig. 5). Therefore, the geographical position of blocking after the warmings (more Atlantic blocks and less blocking over Eurasia) could potentially contribute to reduce the tropospheric forcing of large-scale upward propagating PWs into the stratosphere, particularly for wavenumber 1.
Similar interpretation applies to the Pacific sector. The model simulates a reduced frequency of blocking days over the western part of the region (135°E-195°E) spanning approximately the 15-day PRE-SSW to the 20-day POST-SSW period, which is consistent with amplifying amplitude of PWs 1 and 2 over this region and time-lag (not shown), and the enhanced vertically propagating PWs 1 and 2 (Fig. 5). Over the eastern Pacific, an enhanced blocking occurrence over the climatological pressure ridge within the 20-day window centered around the SSW onset dates is associated with the amplification of the planetary wave ridge (particularly associated with wavenumber 2, not shown) and the enhancement of the upward wavenumber 2 activity flux as seen in Figure 5.
The results presented here show that SSW-related blocking anomalies are part of a large-scale wave structure that tends to enhance the pre-existing climatological-mean planetary wave pattern, and provide further evidence of the dependence between the variability of upward propagating PWs and the geographical position of blocking. An increased (decreased) frequency of blocking over the climatological-mean ridge (trough) is associated with the enhancement of upward propagating PWs into the stratosphere.

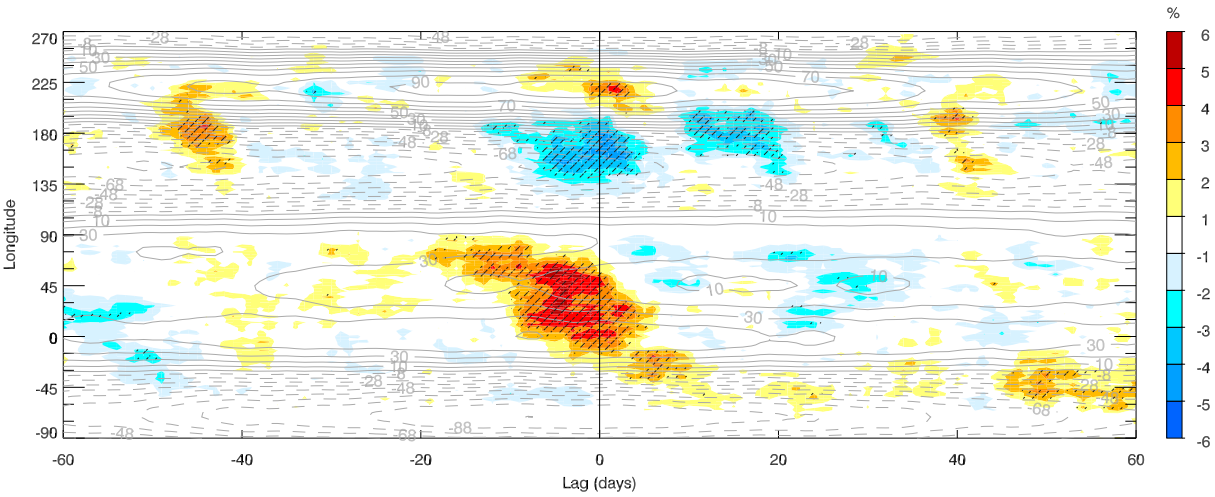

Fig. 6 Temporal evolution of the anomalous frequency of days (in %) within the ONDJFMAM period that are part of large-scale blocking episodes (at least 5-day duration) as a function of longitude (color shading). The anomalous blocking frequency is calculated as the deviation from the daily climatological seasonal cycle, composited for all 480 SSW events, from the 60-day PRE-SSW to the 60-day POST-SSW period. Significant anomalies at the 99% confidence level (based on a T-test) are indicated with black hatching. Grey contours represent the composite of anomalies with respect to the climatological mean of planetary waves 1 to 3 in the 500 hPa geopotential height, averaged between 45°N and 75°N (solid contours are positive anomalies from the climatological mean; dashed contours are negative).

The westward displacement of positive blocking anomalies over the Euro-Atlantic region during the life-cycle of SSWs is an interesting feature that has not been reported in previous studies. To further investigate the anomaly structure of the flow, we show maps of deseasonalized 500-hPa geopotential height anomalies, composited for all SSWs from the 20-day PRE-SSW to the 60-day POST-SSW period (Fig. 7), which reflect well the evolution of blocking anomalies seen in Figure 6.
In the first panel, a weak (but significant) positive height anomaly emerges over Eurasia. At lag = -8 to -1

days (second panel in Fig. 7), this anomaly strengthens and connects up, via the polar region, with another anticyclonic anomaly located over the eastern Pacific. Note that at this time, blocking anomalies over the east Pacific and Eurasian regions are simultaneously simulated by the model (Fig. 6). After the onset, the Pacific anomaly slowly retracts to the pole, while the anomalous Eurasian anticyclone moves westward over the North Atlantic region, on the poleward side of a developing cyclonic anomaly at subtropical/middle latitudes. This high-low dipole anomaly in the geopotential height field over the North Atlantic region persists for about 2 months (panels for days 0-7, 8-15 and 16-59), and mirrors the westward displacement of blocking anomalies over the Euro-Atlantic region seen in Figure 6.

The POST-SSW geopotential height structure seen in Figure 7 strongly projects onto the negative phase of the NAO, as also demonstrated in previous studies (e.g., Baldwin and Dunkerton 2001 and Charlton and Polvani 2007). Because blocking is defined as a reversal of the 500-hPa geopotential height gradient, this anomalous pattern is propitious for more block detections by our index. And so, from a pure methodological aspect, this explains why there can be enhanced blocking over the Atlantic during the negative phase of the NAO. Nevertheless, previous statistically- and dynamically-based studies, exploring the NAO-blocking link, also suggested that the negative phase of the NAO creates an environment favorable for block formation over the North Atlantic region (Barriopedro et al, 2006; Croci-Maspoli et al, 2007; Shabbar et al, 2001).

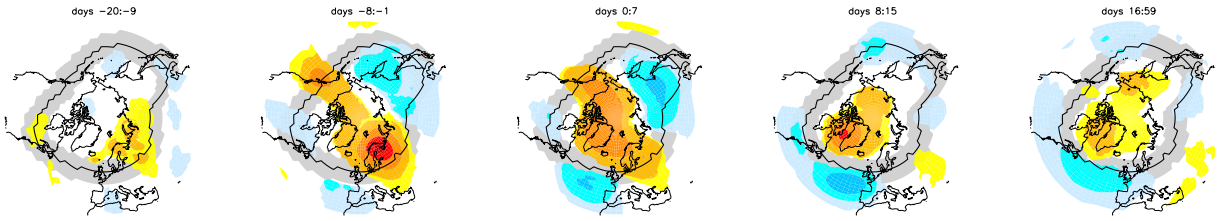

Fig. 7 Averaged daily geopotential height anomalies (from the daily climatological cycle) at 500 hPa spanning the 20-day PRE-SSW to the 60-day POST-SSW period. The length of each averaged period is indicated at the top of each panel. Statistically significant anomalies (at the 99% level, based on a T-test) are displayed by shaded areas with contour intervals at [-50,-45,-40,-30,-20,-10,10,20,30,40,45,50] meters. The solid black line is the reference latitude for identifying blocking, taken as the latitude of the maximum storm track intensity; the grey area represents ±7.5° around the storm track latitude allowed for blocking identification.

4 SSW-related tropospheric blocking climatology

The analysis of SSW-blocking relationships can be biased by the fact that blockings and SSWs have a seasonal cycle (Fig. 3 and 2). Although it was shown in the previous section that the IPSL-CM5A model can reproduce significant deseasonalized SSW-related anomalies in blocking frequency (Fig. 6), we now refine our analysis and testing procedure in order to (1) increase the confidence of our results and (2) assess the dependence between SSWs and blocking persistence.

First, the frequency and persistence of blocking are composited in four different periods (as illustrated in Figure 8) during SSW years only: lag = -40 to -1 days and lag = 0 to +39 days (denoting the 40-day periods preceding and following, respectively, the onset date of SSW events), and lag < -40 days and lag ≥ +40 days (being all the remaining days after the respective 40-day periods). Relatively large periods are defined in order to not exclude long-lasting blocking episodes.

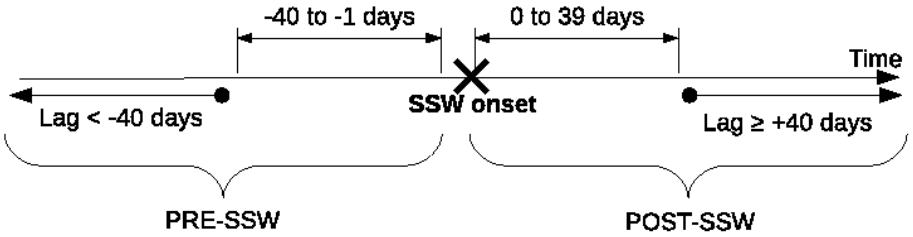

Fig. 8 Schematic representation of the four periods in which the frequency and duration of blocking events are calculated, with respect to the onset date of SSW events (black cross).

Second, and in order to account for the influence of the blocking annual cycle on our results, a Monte Carlo test is performed, whereby blocking frequencies are computed within each of the four periods, with

respect to the same SSW onset dates, but using 480 years randomly selected from the 520 years without any SSW events. The same analysis is performed 500 times, from which a 99% confidence interval is constructed (for each of the four periods). If SSWs have any relationship with blocking variability then the "real results" will lie outside the confidence interval of the 500 random results drawn, with replacement, from years without SSWs.

Results are presented for the blocking frequency (Fig. 9) and duration (Fig. 10). In each case, the red lines show the results for the 40 days immediately before (PRE-SSW) or after (POST-SSW) the onset of SSW, while the black lines are for lag < -40 (PRE-SSW) or lag ≥ +40 (POST-SSW) periods. The red and grey shading are the 99% confidence intervals obtained by randomly drawing data from years without SSWs.

4.1 Blocking frequency

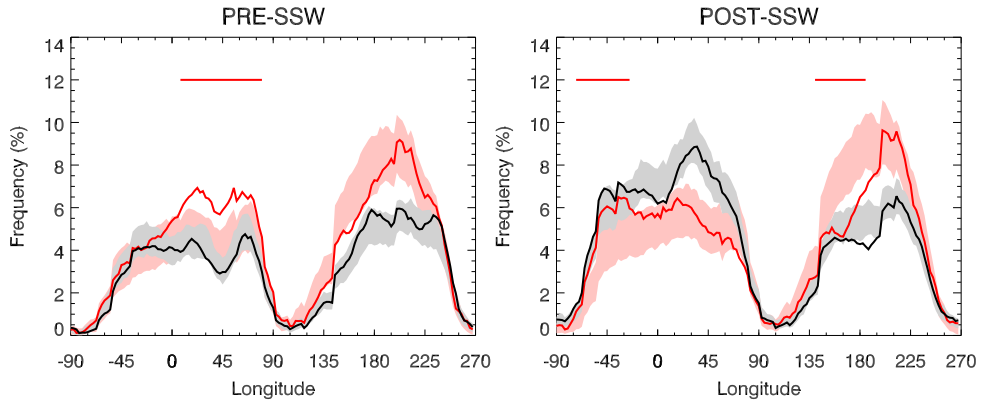

Fig. 9 Frequency of all days that are part of large-scale blocking episodes (at least 5-day duration and 15° longitude extension), as a function of longitude. Red lines are for the 40 days immediately before (left) or after (right) the SSW onset, while black lines are for lag < -40 (left) and ≥ +40 (right) days. The red (grey) shading represents the 99% confidence intervals of blocking frequencies drawn from years without any SSW events for the periods within (more than) 40 days of the SSW onset. The red horizontal lines delineate the regions where the difference between the SSW and non-SSW blocking frequencies, within 40 days of the SSW onset, is significant at the 99% confidence level with the binomial distribution analysis (see description in the text). Note that no black horizontal lines are shown since the binomial analysis shows no significant relationship at lag < -40 days and lag ≥ +40 days.

The tendency of the blocking frequencies computed from the 500 random realizations drawn from years without SSWs (red and black shading in Fig. 9) is comparable to the blocking seasonal cycle seen in Fig. 3 (left panel). This is expected by noting that the four composites (constructed with respect to the SSW onset dates) are also representative of different periods within the seasonal cycle, with October and November days contributing more often to lag < -40 days, December to March days contributing more often to lag = -40 to +39 days, and April and May to lags ≥ +40 days. Following this line of thoughts, Figure 9 shows that non-SSW blocking frequency increases throughout the ONDJFMAM in the Euro-Atlantic region (from lag < -40 days to lag ≥ +40 days), whereas over the Pacific, it first increases toward midwinter: from lag < -40 days (PRE-SSW grey shading) to lag = -40 to -1 days (PRE-SSW red shading), and then decreases toward spring: from lag = 0 to +39 days (POST-SSW red shading) to lag ≥ +40 days (POST-SSW grey shading).

To isolate the dependence of SSWs on blocking frequency from a possible seasonal influence, the blocking frequency computed during SSW years (red and black lines in Fig. 9) can be compared with the non-SSW frequencies (red and grey shading in Fig. 9).

These comparisons show that in the earliest period, more than 40 days prior to the SSW onset, there is no significant SSW-related change in blocking frequency (compare the black line and grey shading in the left panel). In the 40 days before the SSW onset, blocking is significantly more frequent in the Eurasian sector, and slightly (but significantly) less frequent over the west Pacific region (red curve versus shading, in agreement with Fig. 6). However, the occurrence of a SSW event has no significant relationship with Atlantic and eastern Pacific blocks in the PRE-SSW period.

In the POST-SSW period, within the 40 days following SSWs (Fig. 6, right panel, red line versus red shading), the model simulates more frequent Atlantic blocking events and less frequent blocks over the western Pacific. At other longitudes, the frequency during SSW years lies within the 99% range obtained from years without SSW events. At lag > 40 days (black line versus grey shading), there are some longitudes (e.g. near 50°W, 5°E and 180°E) where the SSW blocking frequency is slightly (but significantly) different from the non-SSW range, suggesting that the association between blocking and

stratospheric warming events tends to persist longer than 40 days, as observed in Fig. 6 and reported in other studies (e.g. Thompson et al, 2002). Nevertheless, most of the significant SSW-related signal lies within the period from 40 days prior to 40 days after the SSW onset (particular from lag -20 to lag 20 according to Fig. 6).

Overall, these results confirm that the blocking frequency is significantly related to stratospheric flow disturbances; wintertime blocking frequency is enhanced over the Euro-Atlantic region and reduced in the western Pacific in years when SSW events occur. No significant relationship is found at lags < -40 days and a very weak relationship at lags ≥ +40 days.

As the Monte-Carlo method used to perform the tests in Fig. 9 picks up 500 times 480 years randomly selected, with replacement, out of 520 years without any SSWs, it is not obvious that our random realizations will really be independent of each other. To further test our findings, we have therefore proceeded to a more theoretical test (shown by the horizontal lines in Fig. 9), assuming that each of the blocking frequencies in Fig. 9 is a binomial random variable B, that gives the number of blocked days b out of n independent trials. When the true probability for blocking is p, and n is large we then use the fact that the random variable $(B - np)/\sqrt{np(1-p)}$ is almost normally distributed, and take the 0.5% quantile of the standard normal distribution (i.e., $z_{0.995} = 2.6$) to construct our 99% confidence interval. We then take for p the averaged blocking frequency predicted in years without SSWs and consider that there are around $n = 2000$ truly independent realizations. As there are 480 years without SSWs, this number corresponds to around 4 days per year (separated by a 10-day period) for each of the 40-day periods surrounding the SSWs, which are used to construct the curves shown in Fig. 9. Therefore, instead of using 520x40 days within each of the 4 periods, we consider a decorrelation time of 10 days, in agreement with the fact that the present-day forecast system cannot predict well the weather beyond a week of time lag. The 99% levels are then placed around the p-curves (obtained by averaging the red and grey shading in Fig. 9) at the locations $z = p \pm z_{0.995}\sqrt{\frac{p(1-p)}{n}}$.
The regions delineated by the horizontal lines in Fig. 9 coincide well with the regions identified by the Monte-Carlo test at lag = -40 to +39 days, hence comforting our conclusions there. No significant relationship is found at lags < -40 days and lags ≥ +40 days when we use the binomial test. This new method nevertheless illustrates well that we needed very large samples to arrive at results significant at the 1%-level.

4.2 Blocking duration and planetary waves

The major advantage of the bootstrap method is that it also permits us to test the frequency of large-scale blocking episodes as a function of their duration (i.e., in Fig. 10, using the timing of the SSW onset dates, but with data from random years without SSW events), and assess the changes in the proportion of short and long-lasting blocks between the four different periods.
In the PRE-SSW period, the increase in the frequency of blocking days over the Eurasian sector immediately before the onset of SSW (Fig. 9, left panel), is associated with a significant shift in the distribution of blocking lifetime toward longer blocks (compare the red line and red area in Figure 10, left panel, 2^{nd} row). This does not seem to be the case in the POST-SSW period, where the frequency of blocking days in the lag = 0 to +39-day period over the Atlantic sector is increased (Fig. 6 and 9, right panel), but the frequency of long-lasting blocking episodes (above 11-day duration) tends to decrease, although not significantly (Fig. 10, right panel, 1^{st} row). In the west Pacific sector, blocking tends to be less frequent in lag = 0 to +39-day (and at a lesser extent in lag = -40 to -1 day Fig.9), and this decrease seems to be related to a shift toward shorter blocks (with a stronger signal in the POST-SSW period in Figure 10, right panel, 3^{rd} row).
There are cases where the frequency of blocked days is not significantly affected by the presence of SSW events, but the distribution of blocking lifetime is. In the Atlantic region, for instance, the frequency of lag < -40-day blocking episodes lasting between 8 and 12 days increases significantly (the black line lying outside the 99% confidence interval in Figure 10, left panel, 1^{st} roat lag $\simeq$ 10 to 45 daysw). Similarly over Eurasia, the distribution of lag = 0 to +39-day blocking episodes tends to be shifted toward shorter blocks (Fig. 10, right panel, 2^{nd} row), while no significant changes are found for the overall frequency of blocked days (Fig. 9, right panel).
Overall, it is apparent that an increased (decreased) frequency of blocking days before the onset of SSWs is associated with a shift in the distribution of blocking lifetime toward longer (shorter) blocks (i.e., lag = -40 to -1 days in Eurasia and the west Pacific). However, when the frequency of days is not affected by SSWs, the frequency of long-lasting blocking episodes tend to be at the upper limit of (or even above) the significance level (i.e., for lag = -40 to -1 and lag < -40-day in the Atlantic, lag < -40-day in the west Pacific - except in the eastern Pacific). Interestingly, this does not seem to be the case in the 40 days after

the SSW onset, where blocking durations computed in SSW years tend to be reduced in all sectors following SSWs, relative to blocking durations computed for non SSW years.

This last result can be partly explained by considering each contribution from PW 1 to PW 3 within periods preceding and following the onset date of SSWs, in recognition of the fact that blocking flow is dominated by zonal wavenumbers 1 to 3 (as indicated by observational studies - e.g., Colucci et al 1981). The amplitude of wave disturbances is measured by the root mean squared (hereafter, RMS) geopotential height anomalies, averaged over all longitudes, and computed for each latitude (between 0° and 90°N) and calendar day (spanning the 60-day PRE-SSW to the 60-day POST-SSW period). A Hovmöller representation of the RMS PW anomalies spanning all latitudes can be seen in Figure 11 for wavenumbers 1 (top), 2 (middle) and 3 (bottom), along with their respective latitudinal average between 30°N and 75°N. By taking the RMS of PW anomalies, the amplitude only (not the phase) of PW anomalies are being measured. In that way, the strength of the main wave disturbances (the essential components of the blocking wave signal) related to the life cycle of SSWs is clearly quantifiable.
The results in Figure 11 show that the first major change in wave amplitude for PWs 1 to 3 ranges between 10 and 15 days before onset. Relatively high PW anomalies persist for about 20 days, up to lag = +10 days. This period is then followed by a progressive weakening of PW 1 anomalies, while a more abrupt decrease is observed for PW 2 anomalies, so that between lag = +10 days and lag = +60 days the average strength of PW 1 and 2 anomalies returns to similar values as in the period preceding the amplitude increase at lag = -10 days. However, the amplitude of PW 3 disturbances remains, on average, large after lag = +10 days (compared to the period preceding lag = -10 days). As a result, the contribution of wavenumber 3 to the blocking wave signal is higher in the POST-SSW (after lag = +10 days) than in the PRE-SSW (before lag = -10 days) period, while PW 1 and 2 anomalies recover more rapidly from the breakdown of the stratospheric polar vortex. It is plausible that the increased contribution from wavenumber 3, following the onset of SSWs could be consistent with a change in the proportion of short and long-lasting blocks, with more frequent short-lived blocks at the expense of long-lasting blocking episodes (because of the less stationary nature of wavenumber 3 compared to PWs 1 and 2). Another interesting feature drawn from Figure 11 is a minimum in large-scale PW (i.e., PW 1 and PW 2) variance at 50°N-55°N after the onset of SSWs, being reminiscent of the more contrasted (or more frequent) meridional dipole structures (e.g., high-low dipole blocks) in the POST-SSW than PRE-SSW period, as also shown in Figure 7.

The main conclusion drawn from this analysis is that, in the IPSL-CM5A model, the occurrence of SSWs is linked with enhanced (reduced) wintertime blocking frequency in the Euro-Atlantic (west Pacific) sector, and the proportion of long-lasting blocking episodes tend to be higher before SSW events than after, with, in particular, a significant shift in the distribution of blocking lifetime toward longer wintertime Eurasian blocks in lag = -40 to -1-day and shorter wintertime west Pacific blocks in lag = 0 to +39-day.

5 Conclusion

The focus of this study has been to study the relationship between Northern Hemisphere tropospheric blocking and SSW events in the multi-century IPSL-CM5A coupled climate model. In particular, the precursor role of blockings on SSWs and the stratosphere-leading relationship between SSWs and blockings were explored over the main regions affected by blockings (i.e., the Euro-Atlantic and Pacific sectors). The use of a long climate model simulation provides a much larger sample of SSW events than is available in the recent instrumental/re-analysis period, greatly increasing the power of the statistical analyses to distinguish real effects from the influence of the annual cycle.
The main changes in blocking activity (Fig. 6) and in the mid-tropospheric geopotential height field (Fig. 7) begin about 20 days before the onset date of SSWs over the the Euro-Atlantic and Pacific regions and last for about 60 days following the SSW onset (with intermittent signals in the post-SSW period). The anomalous blocking activity during the life-cycle of SSWs is part of a large-scale wave structure that enhances the pre-existing climatological-mean planetary wave pattern and is assumed to contribute to the variability of vertically propagating PWs. From about 20 days prior to the onset of SSW events, an increased frequency of blocked days over Eurasia and a decreased blocking frequency over the western Pacific region contribute to the enhancement of upward propagating planetary-scale waves (as seen by the strong heat flux anomalies associated with wavenumbers 1 and 2 in Figure 5).
Once the warmings have reached their mature stage, it is well known that easterly and weak westerly winds in the stratosphere inhibit further upward propagation of planetary waves (Charney and Drazin, 1961). In this paper, we also suggest that this reduced vertical flux of wave activity may be due to changes in the PW sources (see for instance Nikulin and Lott, 2010). These changes concern the horizontal distribution of blockings and their duration. More specifically, the enhanced blocking frequency over Eurasia, before the onset of SSWs, is followed by an westward displacement of blocking anomalies over the Atlantic re-

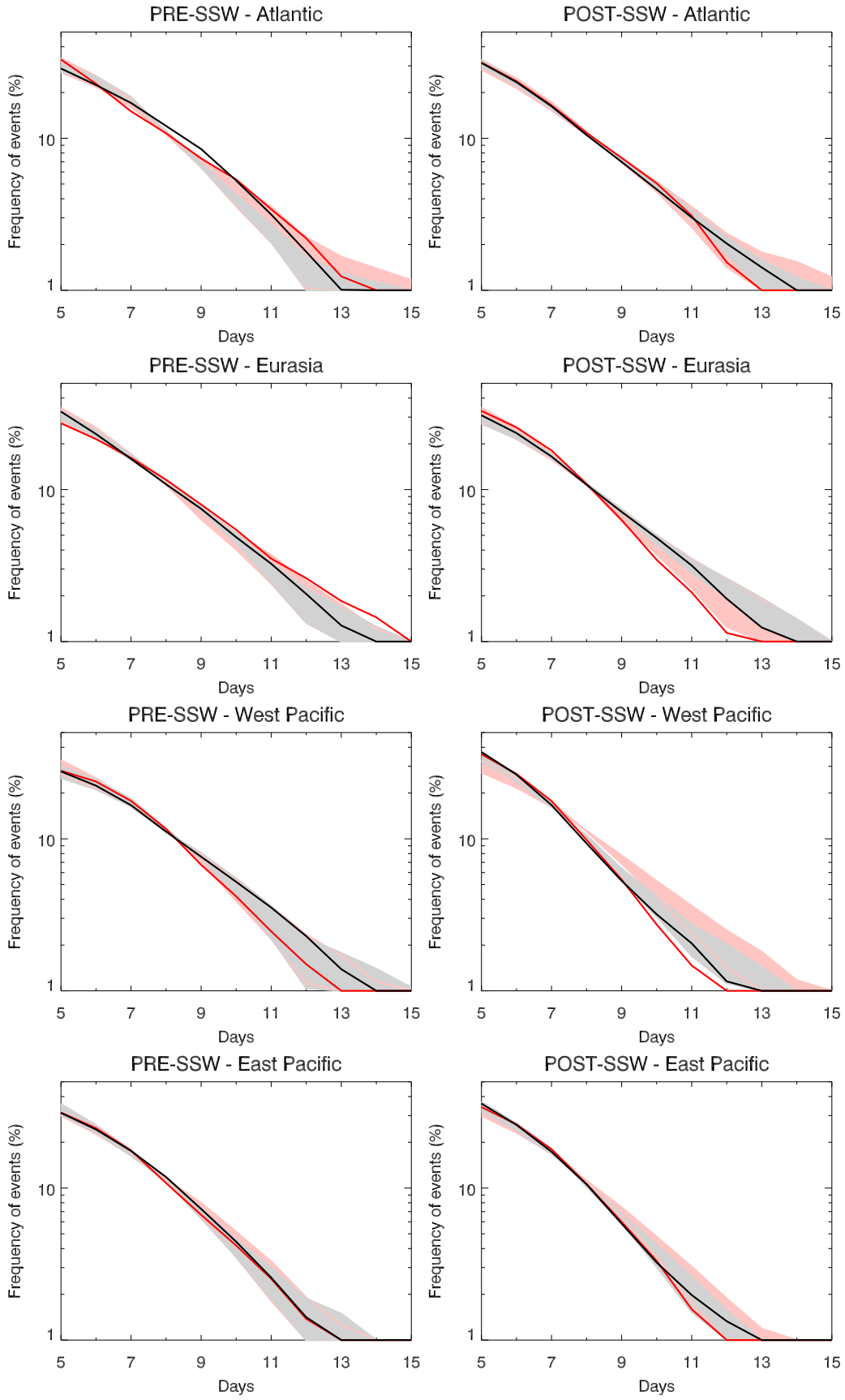

Fig. 10 Blocking duration defined as the average frequency of large-scale blocking episodes (at least 15° longitude extension) as a function of duration (in days) for the Atlantic (75°W-0°, 1^{st} row), Eurasian (0°-75°E, 2^{nd} row), west Pacific (135°E-195°E, 3^{rd} row) and east Pacific (195°E-255°E, 4^{th} row) sectors. Frequencies in the periods preceding the warmings (PRE-SSW) are displayed in the left panels, and the periods following the warmings (POST-SSW) are displayed in the right panels. The red (black) lines are results obtained with "real" SSW events for lag = -40 to -1/lag = 0 to +39-day (lag $<$ -40/lag $\geq$ +40-day) periods and the red (grey) areas represent the 99% confidence interval of the results obtained using model years without SSW events.

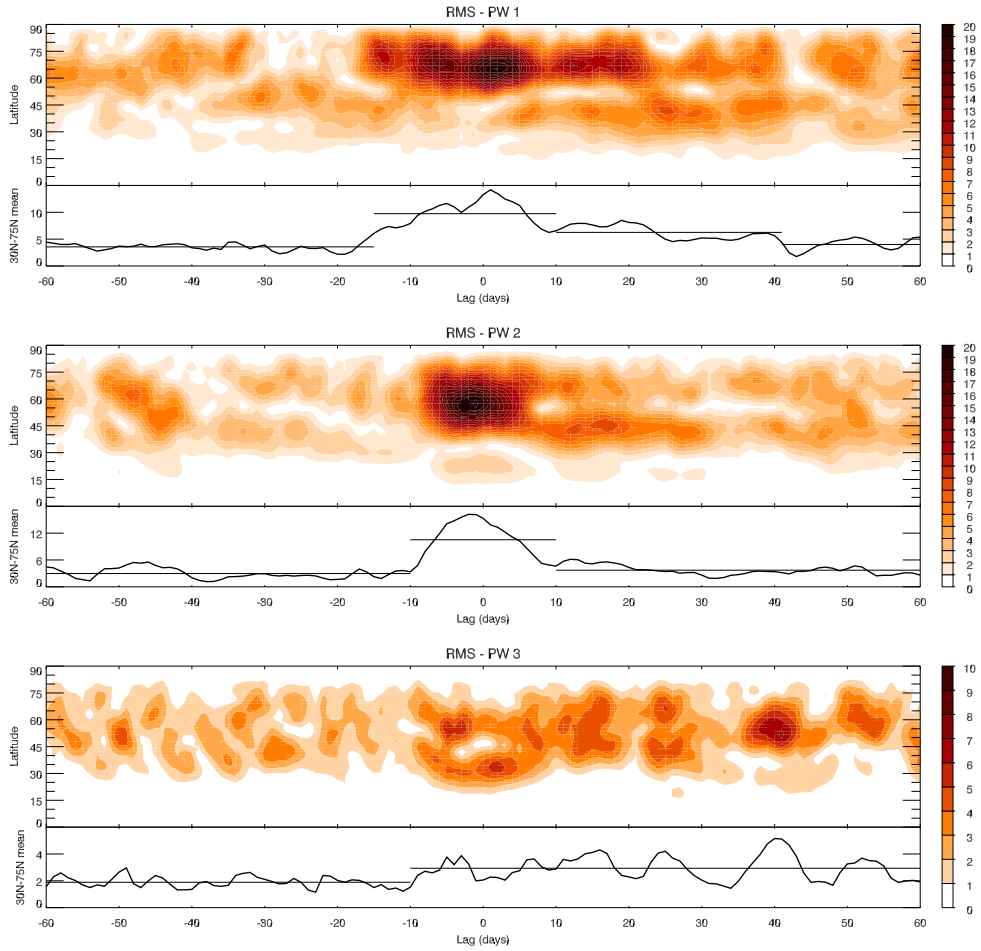

Fig. 11 Latitude-time Hovmöller representation of the root mean squared (RMS) geopotential height anomalies on the 500 hPa geopotential height level, computed for each calendar day, spanning the 60-day PRE-SSW to the 60-day POST-SSW period for wavenumbers 1 (top), 2 (middle) and 3 (bottom). The horizontal (time) axis is shifted with respect the the onset dates of the 480 SSW events (lag = 0 days). The line plot in the lower part of each panel corresponds to the RMS PW anomalies averaged over all latitudes between 30°N and 75°N; the horizontal lines represent time averaged periods. $RMS_l = \sqrt[2]{\frac{1}{N}\sum_{i=0}^{N}(pw_{i,l})^2}$, where $pw_{i,l}$ represents the PW anomaly at a longitude i and lag l from lag = -60 days to lag = +60 days; units are in meters (m).

gion, where lies the climatological-mean planetary trough. As shown in previous studies (e.g., Nishii et al 2011), an increased blocking activity over the climatological-mean planetary trough is associated with decreased PWs. Therefore, in taking into account the geographical location of blockings relative to the phase of climatological-mean planetary waves for the variability of upward propagating PWs (see also Nishii et al 2011), this study assumes that the link between blockings and upward propagating PWs, which is well established prior to the warmings, persists for about two months after the onset of SSWs.

The westward displacement of positive blocking anomalies over the Euro-Atlantic region during the life-cycle of SSWs is a novel result that has not been reported in previous studies. This change in blocking location is associated with a developing high-low dipole geopotential height anomaly over the Atlantic basin, which persists there for about two months after the onset of SSWs. This POST-SSW geopotential height structure, which is reminiscent of the negative phase of the NAO (Baldwin and Dunkerton, 2001; Charlton and Polvani, 2007), creates an environment favorable for the formation of blocking episodes over the North Atlantic region, consistent with previous studies.

The study also shows that the occurrence of SSWs is associated with an enhanced (reduced) wintertime frequency of blocking in the Euro-Atlantic (west Pacific) region (i.e., at $|lag| < 40$ days), while no significant relationship was found at $lag < -40$ days and at $lag > +40$ days (i.e., in autumn and spring, respectively). Finally, SSW-related changes in blocking frequency are associated with a significant shift in the distribution of blocking lifetime toward longer wintertime Eurasian blocks before the warming and shorter wintertime west Pacific blocks after the warming. This latter result is consistent with the fact that prior to SSWs, blocking is dominated by anomalous wave disturbances associated with wavenumber 1 and 2, while following the onset dates of SSWs, the contribution of wavenumber 3 perturbations to the blocking flow is larger.

Acknowledgements This work contributes toward a PhD funded by the School of Environmental Sciences at the University of East Anglia. The authors would like to acknowledge the anonymous reviewers for their helpful comments and suggestions. François Lott was also supported by the EU-FP7 COMBINE project (Grant Agreement number 226520).

References

Ambaum MHP, Hoskins BJ (2002) The NAO troposphere-stratosphere connection. Journal of Climate 15:1969–1978

Andrews DG, Holton JR, Conway BL (1987) Middle atmosphere dynamics, vol 40. Academic Press

Baldwin MP, Dunkerton TJ (2001) Stratospheric harbinger of anomalous weather regimes. Science 294:581–584

Baldwin MP, Thompson DWJ (2009) A critical comparison of stratosphere-troposphere coupling indices. Quarterly Journal of the Royal Meteorological Society 135:1661–1672

Barriopedro D, Garcia-Herrera R, Lupo AR, Hernandez E (2006) A climatology of northern hemisphere blocking. Journal of Climate DOI 10.1007/s00382-010-0767-5

Barriopedro D, Garcia-Herrera R, Trigo RM (2010) Application of blocking diagnosis methods to general circulation models. Part I: a novel detection scheme. Climate Dynamics 19:1042–1063

Charlton AJ, Polvani LM (2007) A new look at stratospheric sudden warmings. Part I: Climatology and modeling benchmarks. Journal of Climate 20:449–469

Charlton-Perez AJ, Baldwin M, Birner T, Black RX, Butler AH, Calvo N, et al (submitted) Mean climate and variability of the stratosphere in the CMIP5 models. Journal of Geophysical Research

Charney JG, Drazin PG (1961) Propagation of planetary-scale disturbances from the lower into the upper atmosphere. Journal of Geophysical Research 66:83–109

Colucci SJ, Loesch AZ, Bosart LF (1981) Spectral evolution of a blocking episode and comparison with wave interaction theory. Journal of the Atmospheric Sciences 38:2092–2111

Croci-Maspoli M, Schwierz C, Davies HC (2007) Atmospheric blocking: space-time links to the NAO and PNA. Climate Dynamics 29:713–725

D'Andrea F, Tibaldi S, Blackburn M, Boer G, Déqué M, Dix M, Dugas B, Ferranti L, Iwasaki T, Kitoh A, Pope V, Randall D, Roeckner E, Straus D, Stern W, Den Dool HV, Williamson D (1998) Northern hemisphere atmospheric blocking as simulated by 15 atmospheric general circulation models in the period 1979-1988. Climate Dynamics 4:385–407

Dole RM, Gordon ND (1983) Persistent anomalies of the extratropical northern hemisphere wintertime circulation: Geographical distribution and regional persistence characteristics. Monthly Weather Review 111:1567–1586

Dufresne JL, al (Submitted) Climate change projections using the IPSL-CM5 earth system model: from CMIP3 to CMIP5. Climate Dynamics

Harnik N (2009) Observed stratospheric downward reflection and its relation to upward pulses of wave activity. Journal of Geophysical Research 114:D08,120

Hourdin F, Foujols M, Codron F, Guemas V, Dufresne J, Bony S, Denvil S, Guez L, Lott F, Ghattas J, et al (2012) Impact of the LMDZ atmospheric grid configuration on the climate and sensitivity of the IPSL-CM5A coupled model. Climate Dynamics pp 1–26

Kodera K, Chiba M (1995) Tropospheric circulation changes associated with stratospheric sudden warmings: A case study. Geophysical Research Letters 100:11,055–11,068

Kolstad E, Charlton-Perez A (2011) Observed and simulated precursors of stratospheric polar vortex anomalies in the northern hemisphere. Climate Dynamics 37:1443–1456

Labitzke K (1965) On the mutual relation between stratosphere and troposphere during periods of stratospheric warmings in winter. Journal of Applied Meteorology 4:91–99

Limpasuvan V, Thompson DWJ, Hartmann DL (2004) The life cycle of the northern hemisphere sudden stratospheric warmings. Journal of Climate 17

Lott F, Fairhead L, Hourdin F, Levan P (2005) The stratospheric version of lmdz: dynamical climatologies, arctic oscillation, and impact on the surface climate. Climate Dynamics

Martius O, Polvani ML, Davies HC (2009) Blocking precursors to stratospheric sudden warming events. Geophysical Research Letters 36

Matsuno T (1971) A dynamical model of the stratospheric sudden warming. Journal of the Atmospheric Sciences 28:1479–1494

Naujokat B, Kruger K, Matthes K, Hoffmann J, Kunze M, Labitzke K (2002) The early major warming in december 2001 - exceptional? Geophysical Research Letters 29(21)

Nikulin G, Lott F (2010) On the time-scales of the downward propagation and of the tropospheric planetary waves reponse to the stratospheric circulation. Annales Geophysicae pp 339–351

Nishii K, Nakamura H, Orsolini YJ (2011) Geographical dependence observed in blocking high influence on the stratospheric variability through enhancement and suppresion of upward planetary-wave propagation. Journal of Climate 24:6408–6423

549 Pawson S, Kubitz T (1996) Climatology of planetary waves in the northern stratosphere. Journal of Geo-
550 physical Research 101:16,987–16,996
551 Pelly J, Hoskins BJ (2003) A new perspective on blocking. Journal of Atmospheric Sciences 60:743–755
552 Polvani LM, Waugh DW (2004) Upward wave activity flux as a precursor to extreme stratospheric events
553 and subsequent anomalous surface weather regimes. Journal of Climate 17:3514–3554
554 Quiroz RS (1986) The association of stratospheric warmings with tropospheric blocking. Journal of Geo-
555 physical Research 91:5277–5285
556 Scaife AA, Woollings TJ, Knight JR, Martin GM, Hinton TJ (2010) Atmospheric blocking and mean biases
557 in climate models. Journal of Climate 23:6143–6152
558 Shabbar A, Huang J, Higuchi K (2001) The relationship between the wintertime North Atlantic Oscillation
559 and blocking episodes in the north atlantic. International Journal of Climatology 21:355–369
560 Taguchi M (2008) Is there a statistical connection between stratospheric sudden warming and tropospheric
561 blocking events? Journal of the Atmospheric Sciences 65:1442–1454
562 Taylor KE, Stouffer RJ, Meehl GA (2012) An overview of CMIP5 and the experiment design. Bulletin of
563 the American Meteorological Society 93(4):485–498, DOI 10.1175/BAMS-D-11-00094.1
564 Thompson DWJ, Wallace JM (2000) Regional climate impacts of the northern hemisphere annular mode.
565 Journal of Climate 13:1000–1016
566 Thompson DWJ, Baldwin MP, Wallace JM (2002) Stratospheric connection to northern hemisphere win-
567 tertime weather: implications for prediction. Journal of Climate 15:1421–1428
568 Tibaldi S, Molteni F (1990) On the operational predictability of blocking. Tellus A 42:343–365
569 Tung KK, Lindzen RS (1979) A theory of stationary long waves. Part I: A simple theory of blocking.
570 Monthly Weather Review 107:714–734
571 Uppala S, Kallberg P, Simmons A, Andrae U, Bechtold VDC, Fiorino M, Gibson J, Haseler J, Hernandez
572 A, Kelly G, Li X, Onogi K, Saarinen S, Sokka N, Allan R, Andersson E, Arpe K, Balmaseda M, Beljaars
573 A, Berg LVD, Bidlot J, Bormann N, Caires S, Chevallier F, Dethof A, Dragosavac M, Fisher M, Fuentes
574 M, Hagemann S, Holm E, Hoskins BJ, Isaksen L, Janssen P, Jenne R, Mcnally A, Mahfouf JF, Morcrette
575 JJ, Rayner N, Saunders R, Simon P, Sterl A, Trenberth K, Untch A, Vasiljevic D, Viterbo P, Woolen J
576 (2005) The ERA-40 re-analysis. Quarterly Journal of the Royal Meteorological Society 131:2961–3012
577 Vial J, Osborn T (2011) Assessment of atmosphere-ocean general circulation model simulations of winter
578 northern hemisphere atmospheric blocking. Climate Dynamics DOI 10.1007/s00382-011-1177-z
579 Woollings TJ, Charlton-Perez A, Ineson S, Marshall AG, Masato G (2010) Associations between strato-
580 spheric variability and tropospheric blocking. Journal of Geophysical Research 115